J Geod (2016) 90:255–262
DOI 10.1007/s00190-015-0870-9

ORIGINAL ARTICLE

Mitigation of multipath effect in GNSS short baseline positioning by the multipath hemispherical map

D. Dong[1] · M. Wang[2] · W. Chen[1] · Z. Zeng[1] · L. Song[1] · Q. Zhang[1] · M. Cai[1] · Y. Cheng[1] · J. Lv[1]

Received: 4 April 2015 / Accepted: 22 October 2015 / Published online: 31 October 2015

Abstract Multipath is one major error source in high-accuracy GNSS positioning. Various hardware and software approaches are developed to mitigate the multipath effect. Among them the MHM (multipath hemispherical map) and sidereal filtering (SF)/advanced SF (ASF) approaches utilize the spatiotemporal repeatability of multipath effect under static environment, hence they can be implemented to generate multipath correction model for real-time GNSS data processing. We focus on the spatial–temporal repeatability-based MHM and SF/ASF approaches and compare their performances for multipath reduction. Comparisons indicate that both MHM and ASF approaches perform well with residual variance reduction (50 %) for short span (next 5 days) and maintains roughly 45 % reduction level for longer span (next 6–25 days). The ASF model is more suitable for high frequency multipath reduction, such as high-rate GNSS applications. The MHM model is easier to implement for real-time multipath mitigation when the overall multipath regime is medium to low frequency.

Keywords GPS · Multipath · Real-time reduction · Spatiotemporal repeatability

1 Introduction

The Global Navigation Satellite System (GNSS) positioning serves a wide variety of applications. Increasing demands push the accuracy of the GNSS positioning to mm level or even high. As the reduction of the other systematic errors makes significant progress in GNSS high-accuracy positioning, the multipath remains one of the primary error sources because it is hard to be parameterized and cannot be eliminated by differencing techniques.

Besides the site selection for less reflective objects surrounding the receiver antenna, efforts to mitigate multipath were made from two categories: hardware-based and software-based approaches. The hardware-based techniques improve the antenna gain patterns to counter the multipath but can only eliminate part of the multipath effects. The software-based methods include developing analytical or simulated multipath models for calibration (Byun et al. 2002), using signal to noise ratio (SNR) in GPS observables (Comp and Axelrad 1998; Lau and Mok 1999; Bilich and Larson 2007), and utilizing various filtering techniques to suppress multipath-dominated frequency band, such as wavelet analysis (Satirapod and Rizos 2005), Kalman filtering (Bernelli-Zazzera et al. 1998) and a Vondrak filter with cross-validation (Zhong et al. 2005; Zheng et al. 2005). Among all the software-based methods, two of them are based on the spatiotemporal repeatability of the multipath under static environment and hence are suitable for real-time multipath reduction. The sidereal filtering (SF) approach (Genrich and Bock 1992; Ragheb et al. 2007a) is based on the repeated constellations of GPS satellites every sidereal day. It is satellite dependent and is realized by observation sidereal lag time (in time domain). The lookup table (Cohen and Parkinson 1991; Fuhrmann et al. 2015), phase map calibration (Hatanaka et al. 2001) and Empirical site model (Moore et al. 2014) approaches are based on the fact of that the multipath relies only on the orbital position in the sky. It is satellite independent and is implemented by grids or spherical harmonics in the sky (in space domain). Aiming at the

✉ W. Chen
wchen@sist.ecnu.edu.cn

[1] Shanghai Key Laboratory of Multidimensional Information Processing, East China Normal University, Shanghai 200241, People's Republic of China

[2] College of Surveying and Geo-Informatics, Tongji University, Shanghai 200092, People's Republic of China

multipath reduction approach suitable for real-time processing, it is instructive to investigate if the two approaches are equivalent, if the satellite dependency is necessary, and what is the advantage and limitation of the two methods.

Since the spatial repeatability is embodied by the spherical positions of satellites on the sky, we call the lookup table method as the MHM (Multipath Hemispherical Map) in this paper to reflect the nature of the model more explicitly. We compare it with the SF approach to gain the insight into the functional behaviors of the multipath effects in space and time domains. Here we focus on the multipath effects of carrier phase observations for high-accuracy applications, such as attitude determination. Our results, however, can be easily extended to the code observations.

2 Multipath characteristics

The received GNSS phase signals are the superposition of electromagnetic waves from direct path and multiple indirect paths of reflective and diffractive effects from surrounding objects, which are called the multipath effects. In most cases the reflective multipath effects are dominant comparing with the diffractive effects. Multipath effects distort the waveform and bias the outputs of phase, code and signal strength.

For phase observables, the multipath-caused phase error ψ is

$$\psi = \arctan\left(\frac{\alpha \sin\gamma}{1+\alpha\cos\gamma}\right) \tag{1}$$

where α is the reflection ratio of amplitude over the direct signal, γ is the phase delay of the reflected signal due to extra path length. The maximum phase error can reach 1/4 wavelength, approximately 4.76 cm for the L1 carrier phase. More details are referred to Hofmann-Wellenhof et al. (2008). For baseline phase difference, the maximum multipath-caused phase error could reach 1/2 wavelength if the phase errors at both ends reach maximum but with opposite signs.

If the satellites are from the same GNSS category (either from GPS or Galileo or Beidou, except Glonass because each Glonass satellite has different signal frequency), from Eq. (1) the ψ relies only on the spherical position of satellite on the sky and is satellite independent. Then the signal from the same hemispherical position generates the same multipath effect to the receiver no matter the signal comes from which satellite. If the multipath environment keeps unchanged, the ψ is further independent of the time for the same spherical position. Such a hemispherical multipath spatial repeatability sets up the foundation of the MHM (or lookup table) approach (Cohen and Parkinson 1991). It stacks the post-processing phase residuals of several days to estimate the mean values for each grid based on the satellite trace in sky. The grid is defined by elevation and azimuth angle either in topocentric coordinate system or carrier coordinate system. In the subsequent days, the estimated grid values are subtracted from the phase observations based on the satellite position in sky. Such a MHM model is baseline and carrier frequency dependent. For different baseline or different carrier frequency, the MHM model should be built by each case.

Since the GPS satellite constellation in sky repeats nearly every sidereal day (23 h 56 m 04 s), the multipath effects also repeat approximately every sidereal day if the reflective environment remains unchanged and the receiver antenna keeps the same. Based on the spatiotemporal repeatability, the sidereal filtering technique was proposed to mitigate the multipath errors (Genrich and Bock 1992; Nikolaidis et al. 2001; Ragheb et al. 2007b). It uses the post-processing phase residuals of several days to estimate the mean values for each satellite at each epoch, the derived values are called 'filter values'. In the subsequent days, the filter values are subtracted from the phase observations based on the same epoch counted in sidereal day interval. By comparing the phase residuals or epoch to epoch site coordinate results between the filtered and unfiltered solutions, we can tell the variance reduction of the SF approach (Ragheb et al. 2007a). This approach requires the filter value subtraction at the same 'sidereal' lag (23 h 56 m 04 s). In practice, however, the observation sample rates are sometimes sparse, for example 30 s. We can only subtract the filter values close to but not exactly at the 'sidereal' lag in the subsequent days. In this case, the efficiency of the SF approach will be reduced.

3 Multipath reduction tests

The carrier phase observable from single antenna is

$$\begin{aligned}\phi^i = {} & \frac{1}{\lambda}[\rho^i(t) + c(\mathrm{d}t - \mathrm{d}t^i) - I + T] \\ & + N^i + \phi_{\mathrm{UPD}} + \phi^i_{\mathrm{mth}} + \varepsilon^i\end{aligned} \tag{2}$$

where i is the satellite index, ϕ^i, ρ^i, N^i, ϕ^i_{mth} are the phase observable, satellite-receiver antenna distance, integer ambiguity, multipath effect related to this satellite, respectively. I and T denote the ionosphere and troposphere effects. $\mathrm{d}t$ and $\mathrm{d}t^i$ denote the receiver and satellite clock errors, respectively. ϕ_{UPD} is the sum of the uncalibrated phase delay (UPD) (Ge et al. 2008) and delays due to hardware bias and cable length, which are satellite independent. ε is the observation noise. The well-modeled, spatially dependent terms such as receiver antenna phase center variation and carrier phase windup effect are not included for clarity.

We set up two antennas on the roof of a building of the East China Normal University campus (Fig. 1). One antenna

Fig. 1 Roof test for the validation of MHM approach

is mounted on a concrete pillar of 0.98 m high. Another antenna is placed on the top of an A/C compressor box of 1.76 m high. The baseline length between the two antennas is about 12.50 m. Both antennas are connected to the Trimble BD982 GNSS receiver, which uses a common receiver clock for the two antennas. Thus, the single difference observations between the two antennas are able to eliminate clock errors from both satellite and receiver simultaneously. In our tests, we use the IGS precise orbit and the between antenna single difference L1 phase observations, so that both satellite and receiver clock errors are canceled out. For short baseline, the effects from troposphere, ionosphere, and phase windup due to satellite antenna rotation are also eliminated. Meanwhile, the satellite orbital errors are almost canceled out for such a short baseline. We place the two antennas towards the same direction to eliminate the effect of receiver antenna phase center variations. Thus, the single difference observation equation becomes

$$\Delta\phi^i(t) = \Delta\rho^i(t) + \Delta N^i + \Delta\phi_{\mathrm{UPD}}(t) + \Delta\phi^i_{\mathrm{mth}}(t) + \varepsilon^i \tag{3}$$

where $\Delta\phi^i$, $\Delta\rho^i$, ΔN^i, $\Delta\phi^i_{\mathrm{mth}}$ are the single difference phase observable, difference of satellite-receiver antenna distances, integer baseline ambiguities and baseline multipath effect related to the satellite, respectively. $\Delta\phi_{\mathrm{UPD}}$ is the differenced UPD between the two antennas. ε is the observation noise. The sampling rate is 1 s and the daily solutions cover full 86,400 s. The Kalman filtering algorithm is adopted and the solutions are solved every second. The tests started from day of the year (doy) 249, 2014 to doy 279, 2014, totally 30 days (due to electric break doy 268 was missing, and doy 269 had only half day observations). All integer ambiguities were resolved successfully using the ambiguity substitution approach (ASA) (Zhou et al. 2015). Parameters of the baseline vector and UPD were first solved. They were tightly constrained in the second run. Then the phase residuals contain only multipath effects, observation noise plus un-modeled and miss-modeled errors.

Our first test examined the spatial repeatability of the multipath effects. The temporal repeatability of the multipath effects is actually deduced from the spatial repeatability. The MHM grids were constructed from the residuals based on the satellite locations on the sky. All grids were defined as the elevation and azimuth angles in topocentric coordinate system. We constructed two 1° by 1° grid MHM models using the residuals from doy 249–251 and doy 252–254, respectively. For GPS satellite with repeat period of about 12 h, such a grid size represents the multipath effects with periods longer than 4 min. The multipath sky maps demonstrate very similar spatial distribution (Fig. 2). Under the environment of our roof test, the multipath effects reach 35 mm level. Relatively larger multipath effects are distributed around 5°–25° ring of the elevation angle, which is consistent with the reflector distribution of the roof environment (Fig. 1).

Our second test searched the best interval to build both MHM and SF models. We set the last 5 days (doy 275–279) data as the multipath reduction target. For each of the last 5 days, we used its previous data of 1–25 days to build the 1° by 1° MHM grid and 1 s sampling SF multipath models, respectively. The SF model is generated based on the sidereal lag epochs of observations. During this period the satellite G09 underwent orbital maneuver, its repeat period demonstrated large and abrupt change (Choi et al. 2004), which affected the efficiency of the SF approach. To be consistent we remove G09 from this and subsequent tests for both MHM and SF models. In this test, we adopt constant values for each grid of MHM approach and use the fixed 'near-sidereal' lag (23 h 55 m 54 s) (Agnew and Larson 2007; Ragheb et al. 2007b) for SF approach. Then we used the models to perform multipath reduction test for the target days and to calculate the residual variance reduction percentage based on the formula of $(1.0 - r_2/r_1) \times 100\ \%$, where r_1, r_2 are the mean residual variances before and after the multipath model correction. Due to the existence of random observation errors,

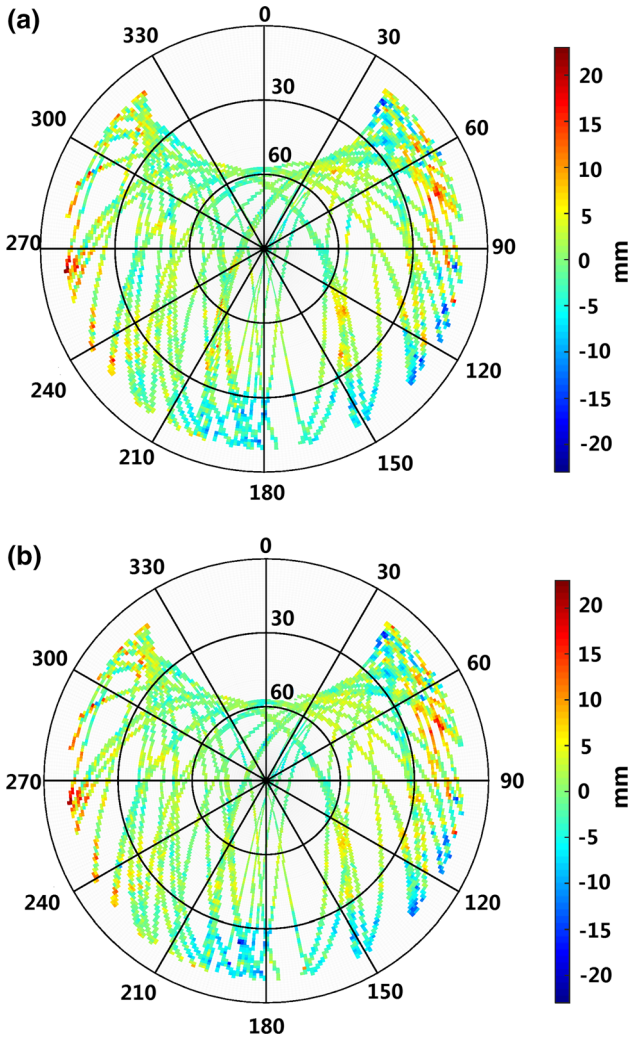

Fig. 2 Sky map of the MHM grid. The azimuth angle is measured clockwise from north. The elevation angle is measured upwards from ground plane. The *center* represents elevation angle 90°. And the *largest circle* represents elevation angle 0°. **a** Model from doy 249–251. **b** Model from doy 252–254

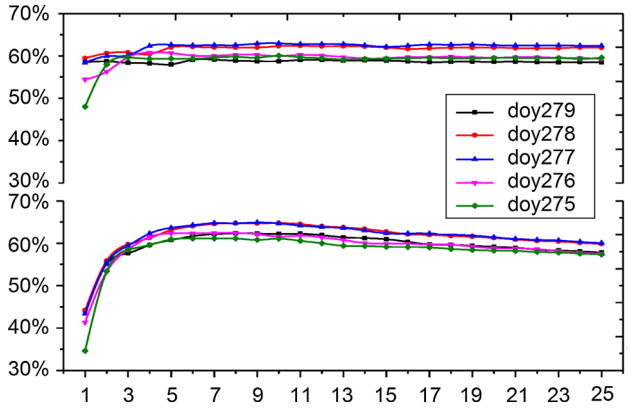

Fig. 3 Residual variance reduction from multipath model correction. *Upper panel* MHM approach; *lower panel* SF approach. *x*-axis unit, day

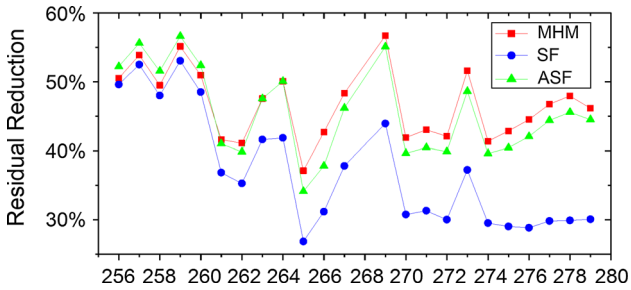

Fig. 4 Comparison of residual variance reduction between the three models. *x*-axis, doy

the reduction percentage cannot reach 100 %, so that the result is considered as the lower bound of the reduction. For MHM model, the reduction percentage increases from 1 day to 5 days then is stabilized at 60 % level (Fig. 3). For SF model, the reduction percentage increases from 1 day to 7 days at the maximum level (about 64 %), and then decreases to 58 % level (Fig. 3), which is consistent with the conclusion of Ragheb et al. (2007b). Since the residual data to build the models include multipath effect and random observation errors, the multi-day average is necessary to suppress the influence of random observation errors. From this test, the best interval appears as 5–7 days.

Our third test adopts first 7 days (doy 249–255) as the interval to build both MHM and SF models. Then we apply the models to perform multipath reduction test for the consequent 23 days (doy 256–279, missing doy 268, doy 269 had only half day observations) (Fig. 4). In this experiment we tested three models. The first two models are the conventional grid with fixed angle increment of the MHM approach and the fixed 'near-sidereal' lag (23 h 55 m 54 s) of the SF approach. Since the actuary satellite repeat period is varying around the 'near-sidereal' lag by ±5 s (Agnew and Larson 2007), to assess the impact of the difference of repeat period on the SF results, our third model is called as the 'advanced SF' (ASF) model, which adopts actual repeat periods for each day and for each satellite, one step further than the mean repeat period of all satellites for each day (Choi et al. 2004). For the first 5 days, the MHM model demonstrates about 50 % variance reduction. After the first 5 days, its variance reduction percentage drops gradually to 45 % level (Fig. 4). The SF model performs similar to the MHM model in the first 5 days at the 50 % reduction level. After 5 days its variance reduction decreases to 30 % level. The ASF model works slightly better than the MHM model in the first 5 days (about 1–2 % more variance reduction). After 5 days its performance is still similar to the MHM model and gradually drops to 45 % level. For the SF model using the accurate orbital repeat period seems critical, in particular it improves the variance reduction significantly for longer term usage (after 5 days).

Figure 5a shows the residuals of satellite PRN 31 before and after the multipath correction at doy 259 for the three models. The unfiltered residual series display low frequency patterns together with high frequency variations. After multipath correction the low frequency patterns are basically eliminated for all the three models. The residual series after corrections become flat and leave mostly high frequency variations. We also perform power spectrum analysis for the four residual time series (Fig. 5b). Power spectrum analysis results indicate that all three models reduce the low frequency multipath effects significantly and the ASF model performs the best reduction. In the high frequency band, the power spectrum maintains similar level before and after corrections and appears nearly flat. One possible reason is that for this test the high frequency multipath effects are not strong and the high frequency variations are mostly from observation noise.

To further understand the nature of the three multipath reduction models, we plot the corresponding model values

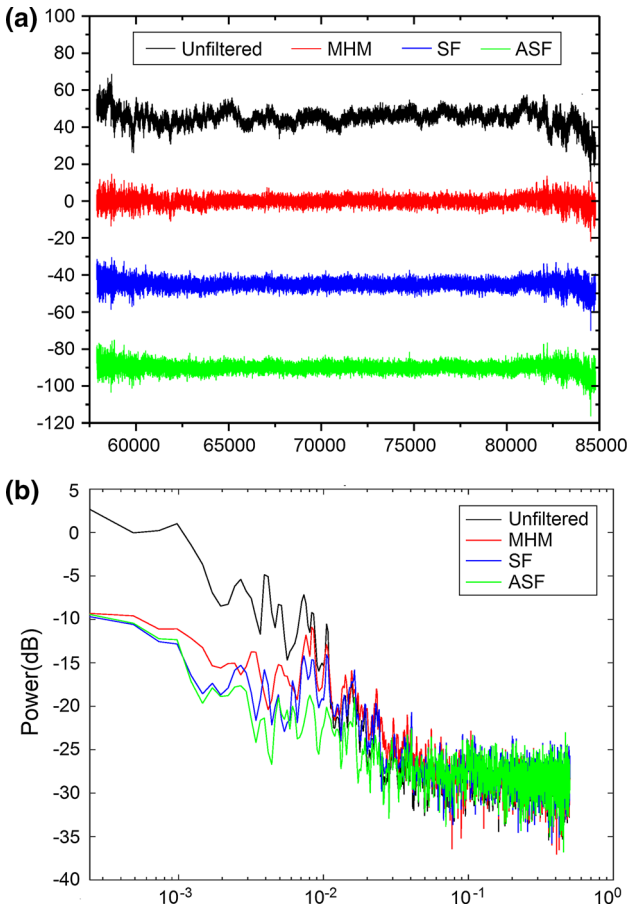

Fig. 5 **a** L1 phase residuals of PRN 31 in doy 259. 45 mm offsets are assigned to separate the four time series. Unit: *x*-axis, second of the day; *y*-axis, mm. **b** Power spectrum density of the four residual time series. Unit: *x*-axis, Hz; *y*-axis, db. *Black curve* before multipath model correction; *red curve* after MHM model correction; *blue curve* after SF model correction; *green curve* after ASF model correction

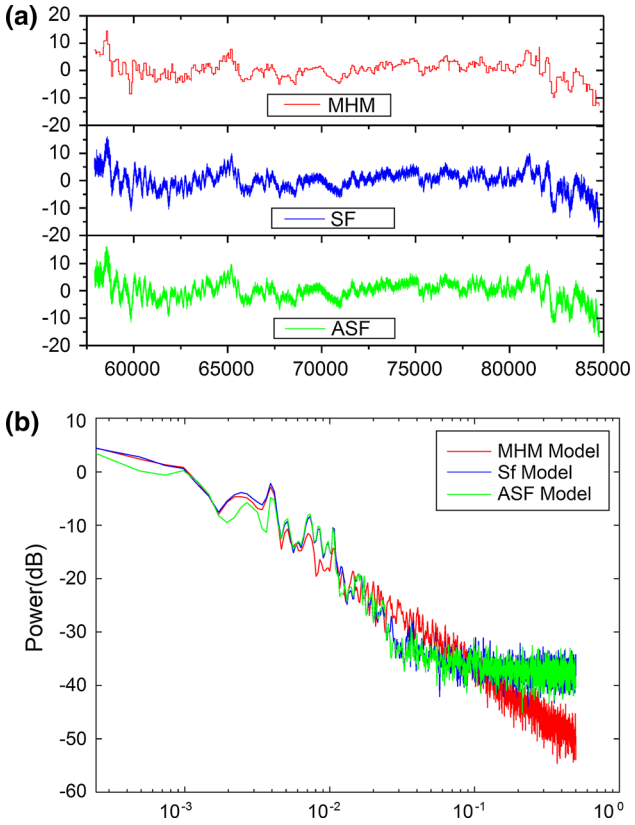

Fig. 6 **a** Multipath reduction models for L1 phase observables of PRN 31 in doy 259. *Upper panel* from MHM 1° by 1° grid model; *middle panel*: from 1 s sampling SF model; *lower panel* from 1 s sampling ASF model. Unit: *x*-axis, second of the day; *y*-axis, mm. **b** Power spectrum density of the three model time series. Unit: *x*-axis, Hz; *y*-axis, db. *Red curve* MHM model; *blue curve* SF model; *green curve* ASF model

for the L1 phase observables of PRN 31 in doy 259 from seconds 58,000 to 84,500 of the day (Fig. 6a). The patterns of the three model series are very similar. But the SF and ASF models have much dense sampling and contains high frequency variations. The MHM model functionally likes a low-pass filter and deducts only low frequency part of the multipath effects (Fig. 6a). Power spectrum analysis also indicates that in low frequency band all three models display similar power and pattern. In the high frequency band (higher than 0.1 Hz), however, the power of the MHM model is much smaller than the SF and ASF models.

Next, we compare the 23 daily baseline solutions with and without applying multipath model correction for ambiguity-free (Fig. 7, right panel) and ambiguity-fixed (Fig. 7, left panel) cases, respectively. The striking feature is that in the ambiguity-free case the solutions without multipath corrections display systematic offsets from the solutions with MHM, SF and ASF model corrections. The offsets are about 2.1, 0.3, 2.1, 1.2 mm for baseline length and north, east, vertical components, respectively (Table 1). The solutions after model corrections are mutually consistent. In the ambiguity-

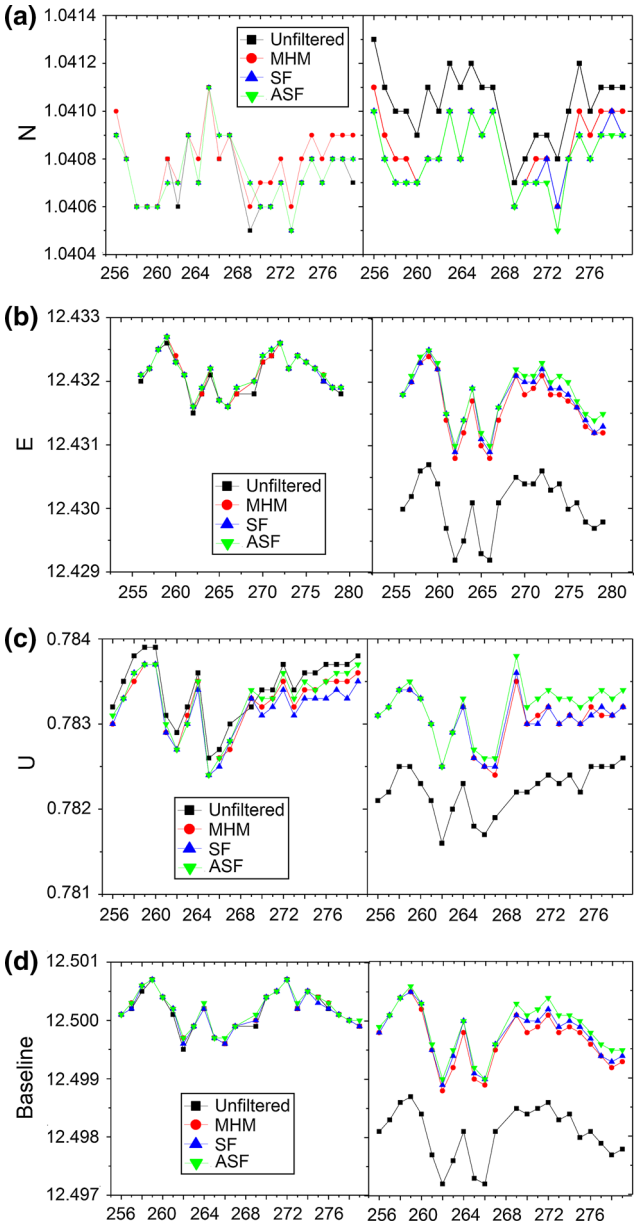

Fig. 7 Comparison of daily baseline solutions with and without applying multipath model correction. *Black curve* without multipath correction; *red curve* with MHM model correction; *blue curve* with SF model correction; *green curve* with ASF model correction. *Left panel* ambiguity-fixed solutions. *Right panel* ambiguity-free solutions. **a** North component; **b** east component; **c** vertical component; **d** baseline length (*x*-axis, doy; *y*-axis unit, m)

fixed case all the solutions before and after corrections agree well to within 0.1 mm level for all 23 days for all baseline length and east, north, vertical components (Table 1). The ambiguity-fixed solutions are also consistent with the ambiguity-free solutions with multipath model corrections. Thus, the major contributions of multipath reduction model to the baseline solutions are in the ambiguity-free case. If the ambiguities are resolved successfully, the four types of

Table 1 Mean values and standard deviations of daily baseline solutions for ambiguity-free and ambiguity-fixed cases with and without applying multipath model correction in Fig. 7

	Unfixed		Fixed	
	Mean	Deviation	Mean	Deviation
Baseline length				
Uncorrected	12.4981	4.51e−4	12.5002	3.29e−4
MHM	12.4997	4.65e−4	12.5002	3.17e−4
SF	12.4998	4.47e−4	12.5002	3.20e−4
ASF	12.4999	4.48e−4	12.5002	3.04e−4
North				
Uncorrected	1.0410	1.46e−4	1.0407	1.35e−4
MHM	1.0409	1.37e−4	1.0408	1.38e−4
SF	1.0408	1.28e−4	1.0407	1.38e−4
ASF	1.0408	1.35e−4	1.0407	1.38e−4
East				
Uncorrected	12.4300	4.52e−4	12.4321	3.15e−4
MHM	12.4316	4.62e−4	12.4321	3.07e−4
SF	12.4317	4.45e−4	12.4321	3.04e−4
ASF	12.4318	4.39e−4	12.4321	3.03e−4
Up				
Uncorrected	0.7822	2.73e−4	0.7834	3.72e−4
MHM	0.7830	2.94e−4	0.7832	3.64e−4
SF	0.7830	2.92e−4	0.7832	3.47e−4
ASF	0.7832	3.21e−4	0.7833	3.76 e−4

Unit: m

baseline solutions agree very well. However, with the help of multipath reduction model the procedure of ambiguity resolution becomes much easier.

To assess the impact of observation sampling rate on the multipath reduction models, we test 5 s sampling records using the above same roof test data from doy 256 to doy 280. In this test, we only compare the residual variance reduction ratio between MHM and ASF models. Both MHM and ASF models were rebuilt using the 5 s sampling data. For comparison we also plot 1 s sampling results in Fig. 8. Comparing with the 1 s sampling results, variance reduction ratio for both models drops 10 % in the 5 s sampling case for the subsequent 5 days and then continues the drop trend to 15 % in doy 280 (Fig. 8). The main reason is that due to the 5 s sampling limitation the accuracy of the satellite orbit repeat period is reduced to 2.5 s level comparing with the 0.5 s accuracy for 1 s sampling data. Also the stacking number in each grid is reduced, which affects the performance of the MHM model.

Finally, we test the multipath reduction models for the observations under strong multipath environment. We set two antennas on the top of a porch in the campus separated by the distance of about 7.60 m. The porch is made of glass and metal and is about 3 m above the ground. Three buildings surround the antennas in the north, east and south directions

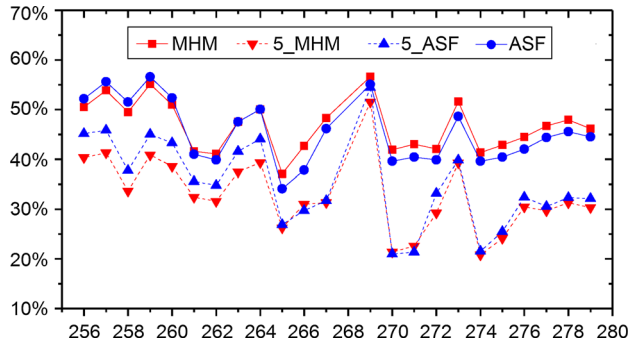

Fig. 8 Comparison of residual variance reduction percentage between the MHM and ASF models. The *red symbols* are MHM model results and the *blue symbols* are ASF model results. *Solid curve* represents 1 s sampling data and *dash curve* represents 5 s sampling data. *x*-axis, doy

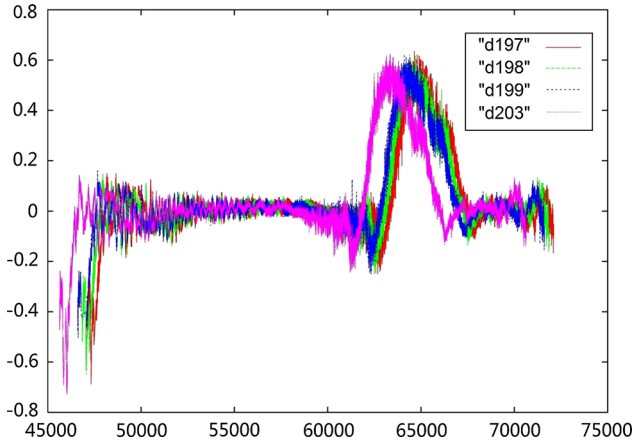

Fig. 9 L1 phase residuals of PRN 15 in doy 197, 198, 199 and 203. Unit: *x*-axis, second of the day; *y*-axis, cycle

with distances of about 5, 30 and 35 m. Such an environment generates strong multipath effects from both near field and far field with both low frequency and high frequency variations. This experiment spanned 11 days from doy 197 to doy 207, 2015. Following the same procedures as the previous experiment, we used the data of first 4 days (doy 197–200) to build the 1° × 1° MHM model and 1 s sampling ASF model. Then we calculated the multipath model generated residual variance reduction ratio for the next 7 days. Figure 9 demonstrates a typical residual series of satellite PRN 15 for doys 197–199 (used to build models) and doy 203 (used to estimate variance reduction ratio). It displayed strong multipath effects with both low frequency and high frequency variations. It also demonstrated clearly the repeated multipath patterns with modified sidereal lag in time domain. In this experiment, more than 85 % of residual variances are significantly reduced for both models, and the reduction ratio of the ASF model (95–92 %) consistently higher than that of the MHM model (90–86 %) (Fig. 10). The reason is that the ASF model is superior over the MHM model for high frequency multipath reduction, and in this experiment

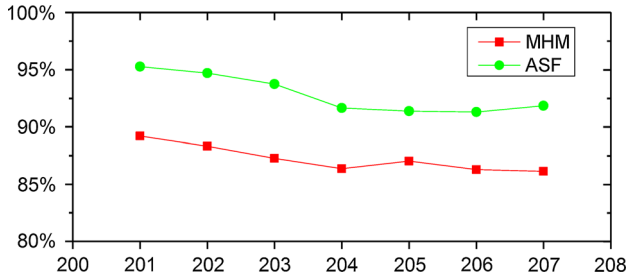

Fig. 10 Comparison of residual variance reduction between the MHM and ASF models. *x*-axis, doy

the high frequency multipath effects are strong. When the high frequency multipath effects vary dramatically within the 1° × 1° grid, one way for the MHM model to absorb the high frequency multipath effect is to reduce the grid size. It is practically hard to build the MHM model with very small grid size. Similar to the previous experiment, both multipath reduction models generated consistent baseline solutions and improved the ambiguity-free solutions. Due to the small sample number (only 7 days) in this experiment, we do not list the corresponding statistics.

4 Discussion and conclusion

Multipath effect is the bottleneck in current GNSS high-accuracy positioning. MHM and SF/ASF are the two software-based approaches, which implement spatiotemporal repeatability of the multipath under static environment and hence are able to build multipath reduction models directly for real-time GNSS data analysis. The MHM correction is realized in space domain (sky grid of orbit trace), while the SF/ASF correction is realized in time domain.

Comparisons of short baseline multipath correction under moderate multipath environment indicate that for short span (next 5 days) both approaches perform similar well in the sense of residual variance reduction (50 % level). For longer span (next 6–25 days) the MHM and ASF models maintain roughly 45 % reduction level, while the reduction of SF model drops to 30 % level. Using accurate satellite-based repeat lag appears important for the SF model, in particular for longer span multipath reduction usage. Sparse sampling rate will reduce the residual variance reduction ratio of both MHM and ASF models. The major contribution of multipath reduction model to the baseline vector solutions is in ambiguity-free case. The improvements of the MHM and SF/ASF models to the baseline solutions are at the same level.

Under strong multipath environment, in particular with strong high frequency multipath variations, both MHM and ASF models are able to reduce most multipath effects.

And the ASF model performs superior to the MHM model because the high frequency multipath effect varies significantly within a grid. Reducing the grid size can help the MHM model to absorb the high frequency multipath effect. However, it is practically hard to build the MHM model with very small grid size. Thus, the ASF model is more suitable for strong high frequency multipath environment, in particular for the high-rate sampling GNSS usage, for example the seismic wave detection.

On the other hand, the MHM model is easier to implement in real-time multipath mitigation. It corrects the multipath effect directly based on the satellite orbital trace in the sky. It avoids to estimate the accurate repeat period of each satellite and to check if the satellite undergoes orbital maneuver in real time. The parameter number of the MHM model is much smaller. Based on the Akaike Information Criterion (AIC) (Bozdogan 1987), both residual variance and adopted parameter number are considered to assess the models. Thus, the MHM model appears more suitable for real-time multipath mitigation. Although in this paper we present the multipath mitigation results of MHM and SF/ASF models for short baseline and phase observables, these spatiotemporal repeatability-based models can be extended to the cases of code observable and single station, if the satellite clock, receiver clock and other terms can be effectively solved. Considering the effectiveness and the broad usage for real-time multipath mitigation, the spatiotemporal repeatability-based methodology, in particular the MHM and ASF approaches, deserves further investigation.

Acknowledgments This work is supported under the contracts of the National Natural Science Foundation of China (No. 61372086, No. 41201380) and Foundation of the Science and Technology Commission of Shanghai (No. 13511500300). We thank editor P. Wills and anonymous reviewers for constructive comments and suggestions.

References

Agnew DC, Larson KM (2007) Finding the repeat times of the GPS constellation. GPS Solut 11(1):71–76

Bernelli-Zazzera F, Campana R, Gottifredi F, Marradi L (1998) GPS attitude determination by kalman filtering: simulation of multipath rejection. AAS 98-199, Breckenridge

Bilich A, Larson KM (2007) Mapping the GPS multipath environment using the signal-to-noise ratio (SNR). Radio Sci 42(6):RS6003

Bozdogan H (1987) Model selection and Akaike's Information Criterion (AIC): the general theory and its analytical extension. Psychometrika 52:345–370

Byun SH, Hajj GA, Yang LE (2002) Development and application of GPS signal multipath simulator. Radio Sci 37(6):10-1–10-23

Choi K, Bilich A, Larson KM, Axelrad P (2004) Modified sidereal filtering: implications for high-rate GPS positioning. Geophys Res Lett 31(22):L22608

Cohen C, Parkinson B (1991) Mitigating multipath error in GPS-based attitude determination. Advances in the astronautical sciences, AAS guidance and control conference, Keystone. Univelt, San Diego, pp 74–78

Comp CJ, Axelrad P (1998) An adaptive SNR-based carrier phase multipath mitigation technique. Trans Aerospace Electron Syst 34(1):264–276

Fuhrmann T, Luo X, Knoepfler A, Mayer M (2015) Generating statistically robust multipath stacking maps using congruent cells. GPS Solut 19:83–92

Ge M, Gendt G, Rothacher M, Shi C, Liu J (2008) Resolution of GPS carrier-phase ambiguities in precise point positioning (PPP) with daily observations. J Geod 82(7):389–399

Genrich J, Bock Y (1992) Rapid resolution of crustal motion at short ranges with the Global Positioning System. Geophys Res Lett 97:3261–3269

Hatanaka Y, Sawada M, Horita A, Kusaka M, Johnson J, Rocken C (2001) Calibration of antenna-radome and monument-multipath effect of GEONET-part 1: evaluation of the phase map by GEONETdata. Earth Planets Space 53:23–30

Hofmann-Wellenhof B, Lichtenegger H, Wasle E (2008) GNSS global navigation satellite systems: GPS, GLONASS. Galileo and more. Springer, Berlin

Lau L, Mok E (1999) Improvement of GPS relative positioning accuracy by using SNR. J Surv Eng ASCE 125(4):185–202

Moore M, Watson C, King M, McClusky M, Tregoning P (2014) Empirical modelling of site-specific errors in continuous GPS data. J Geod 88(9):887–900

Nikolaidis R, Bock Y, Jonge P, Shearer P, Agnew D, Van Domselaar M (2001) Seismic wave observations with the global positioning system. J Geophys Res 106(B10):21897–21916

Ragheb AE, Clarke PJ, Edwards SJ (2007a) Coordinate-space and observation-space filtering methods for sidereally repeating errors in GPS. In: Proceedings of ION national technical meeting 2007, San Diego

Ragheb AE, Clarke PJ, Edwards SJ (2007b) GPS sidereal filtering: coordinate and carrier-phase-level strategies. J Geod 81:325–335

Satirapod C, Rizos C (2005) Multipath mitigation by wavelet analysis for GPS basestation applications. Surv Rev 38(295):2–10

Zheng D, Zhong P, Ding X, Chen W (2005) Filtering GPS time-series using a Vondrak filter and cross validation. J Geod 79(6–7):363–369

Zhong P, Ding X, Zheng D (2005) Study of GPS multipath effects with method of CVVF. Acta Geod Cartogr Sin 34(2):161–167

Zhou F, Dong D, Chen W, Cai M (2015) Isolating fractional phase delays in single differences with common receiver clock. GPS Solut **(submitted)**